



Vibration of FG Porous Three-Layered Beams Equipped by Agglomerated Nanocomposite Patches Resting on Vlasov's Foundation

Mohammad Khorasani¹ · Hassan Elahi² · Marco Eugeni² · Luca Lampani² · Omer Civalek³ 

Received: 24 May 2021 / Accepted: 30 July 2021 / Published online: 6 August 2021
© The Author(s), under exclusive licence to Springer Nature B.V. 2021

Abstract

Equipped sandwich beams (ESBs) are one of the highly demanded structures by the different industries due to their high stiffness to weight ratio. In the present study, the vibrational behavior of a novel ESB is evaluated, analytically. The whole ESB is composed of three layers including functionally graded porous core (FGPC) and two same agglomerated carbon nanofiller reinforced composite (ACNFRC) face sheets. Both nanocomposite layers are constituted from poly(methyl methacrylate) (PMMA) as matrix and CNFs which serve as reinforcing phase. In addition, the effect of agglomeration is considered in nanocomposites, and its tremendous influence on the normalized frequency is depicted in figure and table formats. For the sake of layers properties estimation, power-law and Eshelby–Mori–Tanaka's (EMT)'s approach are hired for, respectively, FGPC and ACNFRCs. Besides this, Hamilton's principle in conjunction with multi-displacement fields and Fourier series analytical method are cooperated tightly to derive motion equations and solve them mathematically. The evaluation of the impacts of various variables as, different displacement fields, thermal environment, CNFs agglomeration, and Vlasov's substrate parameters can be considered as the novelties of this paper. It is revealed that in the context of agglomeration, a higher number of clusters with a lower volume fraction of CNFs inside them can provide higher magnitudes of normalized frequency and consequently rigidity. This work can be assumed as a reference for further future examinations in such a broad context.

Keywords Vibration · Equipped sandwich beam · Carbon nanofillers agglomeration · Multi-shear deformation theory · Vlasov's foundation

✉ Omer Civalek
civalek@yahoo.com

¹ Department of Basic and Applied Sciences for Engineering, Sapienza University, Rome, Italy

² Department of Mechanical and Aerospace Engineering, Sapienza University, Rome, Italy

³ China Medical University, Taichung, Taiwan

1 Introduction

Equipped sandwich structures address at least three-layered structures including a central layer integrated with top and bottom equipped face sheets. Highly progressive demands of different industries for the low weight to strength ratio structures utilization inspired scientists to survey the structures with the capability to satisfy the needs of low weight and high strength requests (Akbaş et al. 2021; Amir et al. 2019a; Civalek et al. 2021; Ge et al. 2021; Le et al. 2021). Therefore, in the passages of years, equipped porous types of sandwich structures' analysis became an interesting field of scholars' research. Moreover, such structures' crucial role in various aspects of manufacturing (costs, stability, durability, etc.) placed them in the central point of scholars' attention more than before. One of the pioneering studies in this context is done by Khatua and Cheung (1973). Their study was about the mechanical behavior of multilayered sandwich beams and plates. Afterward, Maheri and Adams (1994) went further in this context and conducted a study regarding a special type of vibration of the sandwich beams including the honeycomb layer. What's more, considering a porous plate that was saturated, as a model, its lateral vibrational behavior is analyzed by Leclaire et al. (2001). Takahashi and Tanaka (2002) had an investigation about the vibration of imperfect plates. Moreover, Duc et al. (2017) hired first-order shear deformation plate theory (FSDT) von Karman's assumption, Airy stress functions, Galerkin method, and fourth-order Runge–Kutta method, to study the vibration of sandwich composite cylindrical shells with honeycomb core layer. Then, Amir et al. (2020c) examined the buckling behaviors of sandwich plates. For adding more accuracy, the flexoelectric effect is assumed to exist on both face sheets by them. As another attempt, they captured the flexoelectric impact on the vibrational analysis of sandwich plates (Amir et al. 2020c). Furthermore, Babaei et al. (2019) examined thermal buckling and post-buckling responses of geometrically imperfect functionally graded (FG) porous beams based on the physical neutral plane. Fu et al. (2021a) studied the dynamic instability of porous FG conical shells. Their model was exposed to parametric excitation in a thermal environment. Furthermore, they succeed to capture the boundary condition effect on the stability of FG sandwich conical shells (2021b). Soleymani-Javid et al. (2021) conducted a study regarding the vibrational characteristics of sandwich plates. In their honeycomb-based model, various boundary conditions and flexoelectricity effect are taken into account. In another study, Fu et al. (2021c) examined the dynamic instability of laminated FG carbon nanotubes (CNTs) reinforced conical shells. They considered their model rested on the elastic foundations. Also, Kumar and Renji (2019) had a study on the sandwich panels which were composed of honeycomb and composite layers. Their model was subjected to a diffuse acoustic field in a reverberation chamber. Earlier, Sobhy (2020) utilized the differential quadrature method (DQM) for bending analysis of the FG curved sandwich beam. What's more, in addition to the aforementioned attempts regarding sandwich structures, much hardworking is done exclusively, to introduce different types of composite beams, plates, and shells as an unavoidable part of sandwich structures that carry the massive volume fraction of whole sandwich structures' stiffness. As an instance, Amir et al. (2019a) conducted an analytical study on the vibrational behavior of a sandwich FG porous plate. They used quasi-3D tangential deformation plate hypothesis as displacement field, and also, to integrity, they assumed their model in a hygrothermal surrounding and under the force of Lorentz. Also, Fu et al. (2021d) proposed a theoretical model for the eccentrically stiffened composite sandwich cylindrical shell under external mean fluid. Furthermore, Arshid et al. (2020a) handled a study regarding the dynamic and static behavior of

annular FG graphene nanoplatelets (FG-GNPs) reinforced nanocomposite including pores. They considered modified strain gradient theory (MSGT) to take small dimension impacts into account. As another work, Foroutan et al. (2021) examined nonlinear buckling and vibrations of imperfect FG carbon nanofillers (FG-CNFs) reinforced composite cylindrical shells in a hygrothermal environment. In another work, Arshid et al. (2021a) prepared a thermal buckling investigation on the annular/circular microplates. Their model was made of FG graphene nanoplatelets (GNPs) reinforced porous nanocomposite. Further studies are conducted by other scholars in such a broad context (Amir et al. 2020a; Mousavi et al. 2021). Putting such aforementioned simple type of composites aside, nowadays, advanced composite structures are more under evaluation due to their refined mechanical properties. As an example, Moradi-Dastjerdi et al. (2020a) analyzed the buckling behavior of a sandwich plate made of CNTs reinforced porous core patched to two piezoelectric face sheets. They took advantage of the third-order shear deformation plate theory (TSDPT) and Eshelby–Mori–Tanaka’s (EMT)’s approach to handle the motion equations. The most important novelty in their work backs to their CNT agglomeration effects consideration. In addition, Dabbagh et al. (2020a) had an attempt to capture the impacts of CNTs agglomeration on the stability of the nanocomposite beams using refined higher-order beam theories. As another instance, Kamarian et al. (2015) by evaluating CNFs agglomeration impact on the vibrations of a sandwich beam proved that in the most agglomeration states of nanocomposite sandwich beams, the mechanical characteristics become improved due to the presence of agglomerations. Besides strength, another important characteristic of sandwich structures that leads such structures toward popularity is their low weight. So, many scholars move their investigations toward porous layers composed of high-strength materials as functionally graded materials (FGMs). Among them, Fu et al. (2020) investigated thermoacoustic variations of a FG cylindrical shell containing pores. Moreover, Van et al. (2020) investigated nonlinear transient behavior of porous FGM plates. Their model was under hygrothermal and mechanical loads affection. Some other applications of nano- and macroscaled beams can be found in the literature (Avcar 2019; Zenkour and Radwan 2021, 2020; Lazreg and Avcar 2021a, 2021b; Daikh and Zenkour 2019; Jalaei and Civalek 2019; Zenkour 2008, 2018, 2020; Demir and Civalek 2017; Barati and Zenkour 2017).

Keeping mentioned papers in mind, the authors decided to examine the vibrational responses of an equipped sandwich beam (ESB) including FG porous core (FGPC) patched to the two same agglomerated CNFs reinforced composites (ACNFRCs) at the top and bottom. So, in the present study, the vibrational behavior of a novel equipped sandwich beams is evaluated. The sandwich structure is placed on the Vlasov’s substrate and also, under the thermal environment affection. By Hamilton’s principle, Navier’s solution technique, and CNFs’ agglomeration effect consideration, governing equations are gained and solved analytically. Finally, response variations against various parameters’ changes are depicted in the results portion. Based on the present study results, designing and producing different equipments become possible, and also, a higher ratio of stiffness to weight is accessible more than before. Furthermore, considering CNFs’ agglomeration effect on the vibrational behavior of such a model is one of the novelties of this study.

Furthermore, our two-parameter Vlasov’s foundation model included the advantages of the Winkler foundation model and the Pasternak foundation model, and two independent elastic constants are used to represent the characteristics of the given elastic substrate.

2 ESB Analytical Modeling

2.1 Geometrical Information

An ESB with length a and total thickness h is considered as a model to evaluate its vibrational responses due to the different variables' variations. As it is displayed in Fig. 1, the ESB is composed of three layers; FGPC and two identical ACNFRC face sheets. The thickness of the FGPC, top ACNFRC, and bottom ACNFRC is demonstrated by the signs h_c , h_p and h_b , respectively, and their summation denotes ESB total elevation (h). The Cartesian coordinate system (x, y, z) is attached to the imaginary mid-plane of ESB where x and z axes are along with the model's length and thickness directions, one after another. Furthermore, the whole structure is placed on the Vlasov's substrate as an elastic foundation, and also, it is under thermal environment affection.

2.2 General Equations

For the sake of integrity, various displacement field theories are used in this work. So, the ESB's general displacement field can be defined as (Arshid and Amir 2021; Khorasani et al. 2021):

$$\begin{aligned}
 U(x, z, t) &= u(x, t) - zw_{,x}(x, t) + f(z)u_1(x, t), \\
 V(x, z, t) &= 0, \\
 W(x, z, t) &= w(x, t)
 \end{aligned}
 \tag{1}$$

where u and w denote longitudinal and transverse movement components of mid-surface. The term u_1 is the beam rotation representative. Furthermore, subscript comma (\cdot) is the derivative sign, and $f(z)$ is the considered shape function which denotes the transverse shear stress distribution along the z -direction (Sayyad and Ghugal 2019). By the means of

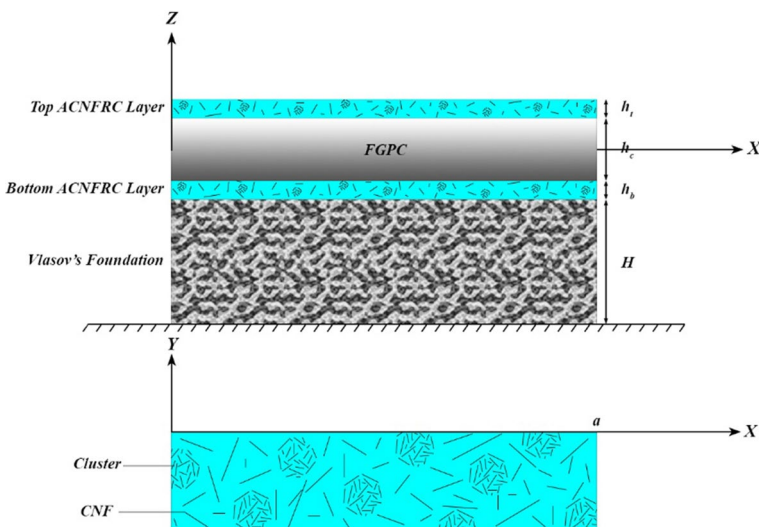


Fig. 1 Configuration of the ESB model

shape function, sufficient flexibility becomes available to switch among different types of displacement fields as is mentioned in Table 1 (Şimşek and Reddy 2013).

Where SSDT, HSDT, and ESDT refer to the sinusoidal, hyperbolic, and exponential shear deformation theories. Also, to address the Timoshenko beam model, the displacement component along x -direction should be considered as $(x, z, t) = u(x, t) + zu_1(x, t)$. In the case of Timoshenko beam model utilization, a shear correction factor equals to $5/6$ is considered.

The strain tensor of under evaluation model can be obtained as (Arshid et al. 2021b):

$$\begin{bmatrix} \epsilon_{xx} \\ \gamma_{xz} \end{bmatrix}^{c,t,b} = \begin{bmatrix} U_{,x} \\ U_{,z} + W_{,x} \end{bmatrix} \tag{2}$$

In which, superscript $c, t,$ and b address the words core, top, and bottom layer.

Stress–strain equations for each of the three layers are identical, whereas the properties vary layer to layer. Stress field can be presented as (Arshid et al. 2020b; Khorasani et al. 2020):

$$\begin{bmatrix} \sigma_{xx} \\ \tau_{xz} \end{bmatrix}^{c,t,b} = \begin{bmatrix} S_{11} & 0 \\ 0 & S_{55} \end{bmatrix}^{c,t,b} \begin{bmatrix} \epsilon_{xx} - \theta \Delta T \\ \gamma_{xz} \end{bmatrix}^{c,t,b}, \tag{3}$$

where S and θ serve as an elastic constant and thermal expansion coefficient, respectively.

Besides this, ΔT is the temperature difference and can be specified as $\Delta T = T(z) - T_{ref}$.

In which T_{ref} denotes the reference temperature which is equal to ambient temperature (293) and $T(z)$ represents temperature variation across the ESB’s height and, in the linear format, it can be addressed as (Tang and Ding 2019):

$$T(z) = T_b + \Delta T_{tb} \left(0.5 + \frac{z}{h} \right) \tag{4}$$

In which, T_b is the ESB’s bottom surface temperature, and also, it is considered as the reference temperature in the current study. Moreover, ΔT_{tb} stands for the temperature difference between ESB’s top and bottom surfaces (i.e., $\Delta T_{tb} = T_t - T_b$).

2.3 ACFRC Face Sheets’ Properties.

Generally, the philosophy of CNFs’ utilization in a polymeric matrix is to improve the mechanical properties of the structure. As the elasticity modulus of the reinforcing phase is much more than the matrix, a polymeric matrix that is reinforced by CNFs has improved mechanical properties in comparison with the pure matrix.

Table 1 The various shape functions corresponding to the different displacement fields (Şimşek and Reddy 2013)

$f(z)$	Displacement field
$\frac{h}{\pi} \sin\left(\frac{\pi z}{h}\right)$	SSDT
$h \sinh\left(\frac{z}{h}\right) - z \cosh\left(\frac{1}{2}\right)$	HSDT
$z \exp\left(-2\left(\frac{z}{h}\right)^2\right)$	ESDT

Despite the mentioned high stiffness, CNFs’ high level of aspect ratio results in their low level of bending strength. As a consequence, CNFs pose a great tendency to be bundled together and form some CNFs concentrated spherical inclusions named clusters. The mentioned effect serves as an agglomeration effect which plays a constructive role in the composite layers’ mechanical properties refinement. On the other hands, CNFs can also be distributed in the matrix without being concentrated in clusters. Therefore, there are two different types of CNFs’ in the polymeric matrix. By definition, μ and η specify the CNFs concentrated region volume fraction and the sprinkled CNFs inside the clusters volume fraction as (Dabbagh et al. 2020a):

$$\begin{aligned} \mu &= V^{\text{Cluster}} / V \\ \eta &= V_r^{\text{Cluster}} / V_r \end{aligned} \tag{5}$$

In which, V is a sign to illustrate the representative volume element (RVE), V^{Cluster} addresses the net volume of CNFs concentrated regions inside the borders of RVE, V_r^{Cluster} denotes the total volume of CNFs inside the clusters, and the term V_r implies the net volume of CNFs inside the RVE. It should be noticed that the magnitude of μ in the maximum case is equal to η . To provide a clear physical imagination for the abovementioned parameters, it is worthwhile mentioning that:

- μ equal to zero specifies non-agglomerated layer which means there is no concentration of CNFs in the CNFRCs. On the other hands, when its value is equal to one, the whole composite layer serves as a big agglomerated region.
- Considering the abovementioned methodology limitation ($\eta \geq \mu$), η equal to zero implies there is no CNF inside the clusters, so basically there is no cluster. While η equal to one denotes all CNFs are accumulated inside the clusters and ACNFRCS contain no CNF out of the clusters.
- In a specific case, when $\mu = \eta = 1$, there is fully CNFs agglomerated composite.

For the sake of ACNFRCS’ mechanical properties capturing, the Eshelby–Mori–Tanaka technique (EMTT) is hired (Shi et al. 2004). Based on the EMTT, the bulk modulus (K) and the shear modulus (G) inside and outside of the clusters can be defined as (Moradi-Dastjerdi et al. 2020b; Shi et al. 2004):

$$K_{in}^{t,b} = K_p + \left((\delta_r - 3K_p\alpha_r) f_r^{t,b} \eta / 3 (\mu - f_r^{t,b} \eta + f_r^{t,b} \eta \alpha_r) \right), \tag{6}$$

$$G_{in}^{t,b} = G_p + \left((\eta_r - 2G_p\beta_r) f_r^{t,b} \eta / 2 (\mu - f_r^{t,b} \eta + f_r^{t,b} \eta \beta_r) \right), \tag{7}$$

$$K_{out}^{t,b} = K_p + \left((\delta_r - 3K_p\alpha_r) f_r^{t,b} (1 - \eta) / 3 ((1 - \mu) - f_r^{t,b} (1 - \eta) + f_r^{t,b} (1 - \eta) \alpha_r) \right), \tag{8}$$

$$G_{out}^{t,b} = G_p + \left((\eta_r - 2G_p\beta_r) f_r^{t,b} (1 - \eta) / 2 ((1 - \mu) - f_r^{t,b} (1 - \eta) + f_r^{t,b} (1 - \eta) \beta_r) \right) \tag{9}$$

where subscripts p , r , and the term f_r address the polymeric matrix, CNFs reinforcing phase, and the total volume fraction of CNFs inside the composite. The evaluation of the vibrational response of the current ESB due to the various types of CNFs distribution

through the polymeric matrix is accessible by the means of following CNFs volume fraction equations as (Amir et al. 2019b):

$$f_r^{t,b} = \begin{cases} f^* & U \\ \frac{4}{h_{r,b}} \left| z \mp \frac{h_c+h_{t,b}}{2} \right| f^* & FG - X \\ 2 \left(1 - \frac{2}{h_{r,b}} \right) \left| z \mp \frac{h_c+h_{t,b}}{2} \right| f^* & FG - O \\ \left(1 - \frac{2}{h_{r,b}} \right) \left(z \mp \frac{h_c+h_{t,b}}{2} \right) f^* & FG - A \\ \left(1 + \frac{2}{h_{r,b}} \right) \left(z \mp \frac{h_c+h_{t,b}}{2} \right) f^* & FG - V \end{cases} \quad (10)$$

In Fig. 2, the variation of CNFs volume fraction versus composite layer thickness is displayed for different types of CNFs distribution.

What's more, the terms α_r , β_r , η_r and δ_r can be written as follows (Moradi-Dastjerdi et al. 2020a):

$$\alpha_r = (3(K_p + G_p) + k_r - l_r) / 3(G_p + k_r), \quad (11)$$

$$\beta_r = 0.2 \left[\frac{4G_p + 2k_r + l_r}{3(G_p + k_r)} + \frac{4G_p}{G_p + p_r} + \frac{2\{G_p(3K_p + G_p) + G_p(3K_p + 7G_p)\}}{G_p(3K_p + G_p) + m_r(3K_p + 7G_p)} \right], \quad (12)$$

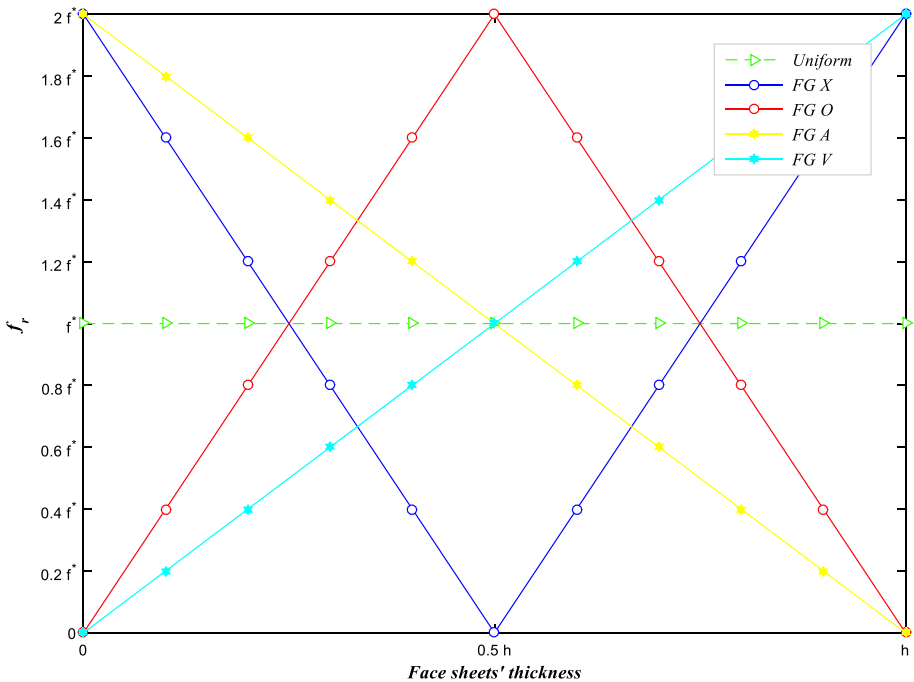


Fig. 2 The variation of CNFs volume fraction versus thickness of composite face sheets for different types of CNFs distribution

$$\eta_r = 0.2 \left[\begin{aligned} & 0.66(n_r - l_r) + \frac{8G_p p_r}{G_p + p_r} + \frac{8G_p m_r (3K_p + 4G_p)}{3K_p (G_p + m_r) + G_p (G_p + 7m_r)} \\ & + \frac{2(k_r - l_r)(2G_p + l_r)}{3(G_p + k_r)} \end{aligned} \right], \quad (13)$$

$$\delta_r = 0.33 \left[n_r + 2l_r + \frac{(2k_r + l_r)(3K_p + 2G_p - l_r)}{G_p + k_r} \right] \quad (14)$$

At the current equations k_r , l_r , m_r , p_r and n_r address the CNFs' elastic Hill's constants which are varied for various types of CNFs concerning their chiral index magnitude. In the current study mentioned constants related to single-walled carbon nanofillers (SWCNFs) with a chirality index equal to 10 are used (Fantuzzi et al. 2017).

So, the thickness-dependent bulk modulus and the shear modulus of the ACNFRs are obtained by the means of EMTT as (Dabbagh et al. 2020b):

$$K_n^{t,b}(z) = K_{out}^{t,b} \left\{ 1 + \mu \left(\frac{K_{in}^{t,b}}{K_{out}^{t,b}} - 1 \right) / \left(1 + \alpha^{t,b} (1 - \mu) \left(\frac{K_{in}^{t,b}}{K_{out}^{t,b}} - 1 \right) \right) \right\}, \quad (15)$$

$$G_n^{t,b}(z) = G_{out}^{t,b} \left\{ 1 + \mu \left(\frac{G_{in}^{t,b}}{G_{out}^{t,b}} - 1 \right) / \left(1 + \beta^{t,b} (1 - \mu) \left(\frac{G_{in}^{t,b}}{G_{out}^{t,b}} - 1 \right) \right) \right\} \quad (16)$$

In which subscript n denotes nano ACNFRs and:

$$\alpha^{t,b} = (1 + v_{out}^{t,b}) / 3(1 - v_{out}^{t,b}) \quad (17)$$

$$\beta^{t,b} = 2(4 - 5v_{out}^{t,b}) / 15(1 - v_{out}^{t,b})$$

And

$$v_{out}^{t,b} = (3K_{out}^{t,b} - 2G_{out}^{t,b}) / (6K_{out}^{t,b} + 2G_{out}^{t,b}) \quad (18)$$

Finally, the elastic modulus (E), Poisson's ratio (ν) density (ρ) and thermal expansion coefficient (θ) of the nano ACNFRs can be simulated as (Kamarian et al. 2016; Moradi-Dastjerdi et al. 2020a):

$$E^{t,b}(z) = 9K_n^{t,b} G_n^{t,b} / (3K_n^{t,b} + G_n^{t,b}), \quad (19)$$

$$\nu^{t,b}(z) = (3K_n^{t,b} - 2G_n^{t,b}) / (6K_n^{t,b} + 2G_n^{t,b}), \quad (20)$$

$$\rho^{t,b}(z) = (\rho_r^{t,b} - \rho_p^{t,b}) f_r^{t,b} + \rho_p^{t,b}, \quad (21)$$

$$\theta^{t,b}(z) = \left(\frac{E + 4\nu K_n(1 + \nu)}{E + 4K_n(1 + \nu)^2} \right)^{t,b} \left(\frac{f_r^{t,b} E_{11}^{CNF} \theta_{11}^{CNF} + (1 - f_r^{t,b}) E_p \theta_p}{f_r^{t,b} E_{11}^{CNF} + (1 - f_r^{t,b}) E_p} \right) \tag{22}$$

The elastic constants for top and bottom face sheets are identical in the formulation as (Zhang et al. 2021):

$$\begin{bmatrix} S_{11}(z) \\ S_{55}(z) \end{bmatrix}^{t,b} = \begin{bmatrix} E(z)(1 - \nu^2(z))^{-1} \\ 0.5E(z)(1 + \nu(z))^{-1} \end{bmatrix}^{t,b} \tag{23}$$

2.4 FGPC Properties

As mentioned before, the ESB’s core is an imperfect layer that is made of FGMs. So, the top and bottom surfaces of the FGPC are assumed to be pure ceramic and pure metal. To add more elaboration in this context, three different types of imperfection dispersions are taken into account and their impact on the mechanical behavior of the whole sandwich model is compared to each other. Based on the rule of the mixture in its imperfection-dependent format, the FGPC’s mechanical properties in the case of uniform porosity dispersion can be defined by the following formulation (Kumar et al. 2021):

$$R^c(z) = (R_c - R_m) V_c + R_m - (R_c + R_m) \frac{e}{2} \tag{24}$$

where R is the sign to address different mechanical properties as $E, \nu, \rho,$ and θ . Also, subscripts c and m are used to distinguish ceramic properties and metallic properties. Furthermore, e denotes porosity index, and V_c stands for ceramic volume fraction which can be presented as (Dastjerdi et al. 2020):

$$V_c(z) = \left(0.5 + \frac{z}{h_c} \right)^n, V_c = 1 - V_m \tag{25}$$

In which, n is the power-law index, gradient index, or material property exponent. Based on the aforementioned equation, the ceramic and metal volume fractions variation versus core thickness is plotted in Fig. 3 for various material property exponents.

As it is visible in Fig. 3, the power-law index enhancement results in ceramic volume fraction increasing at a lower rate across the first half-thickness of the core (Akgöz and Civalek 2014).

The core mechanical properties in the case of X type dispersion of porosities can be presented as (Fan et al. 2021):

$$R^c(z) = (R_c - R_m) V_c + R_m - (R_c + R_m) \left| \frac{2z}{h_c} \right| \frac{e}{2}, \tag{26}$$

And finally, dispersing porosities within the FGPC based on the O pattern result in the following model for FGPC’s mechanical properties capturing as (Thanh et al. 2019):

$$R^c(z) = (R_c - R_m) V_c + R_m - (R_c + R_m) \left\{ 1 - \left| \frac{2z}{h_c} \right| \right\} \frac{e}{2}, \tag{27}$$

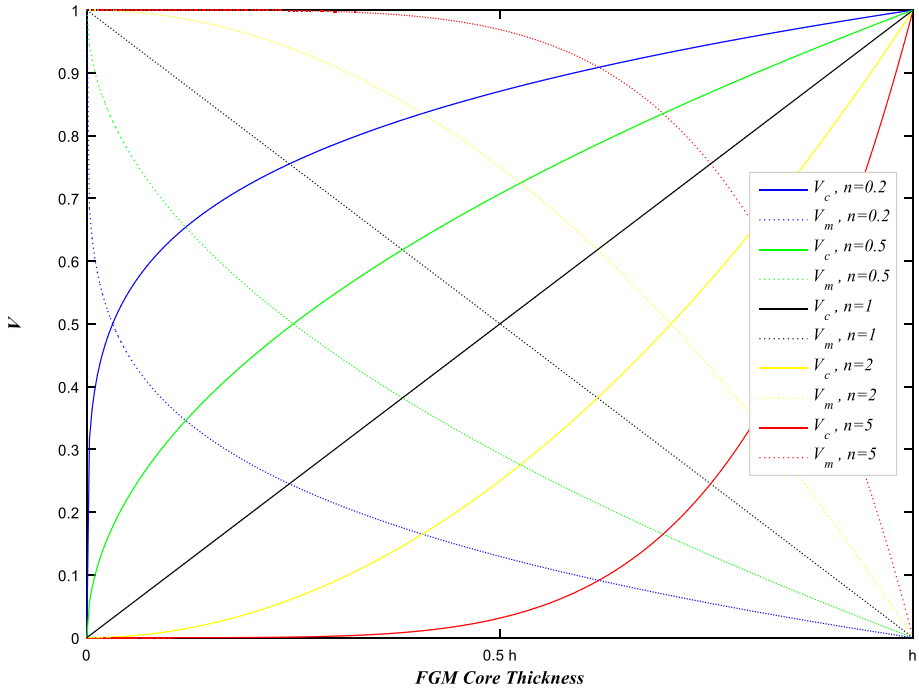


Fig. 3 The variation of ceramic and metal volume fractions versus core thickness for different power-law indexes

Also, it seems to be mandatory to mention that setting e equal to zero in each type of pores dispersion causes having perfect FGC instead of the FGPC.

To provide a more comprehensive physical mental background about FGPC and based on Eqs. (24, 26 and 27), the FGPC's elastic moduli variation against its thickness is plotted as it is visible in Fig. 4. As curves say, passing from the core bottom surface to the top surface, the FGPC's elastic modulus for all types of porosity dispersion increases, by and large. Such behavior is due to the high elastic modulus of ceramic over metal. Another noticeable point is that in this figure, there are three important points; i.e., $z = 0, \frac{h}{2}$ and h . As it is obvious, at the top and bottom surface of FGPC, the elastic modulus related to the curves perfect FGC and O-FGPC has the same values. Also, there is a similar attitude regarding U-FGPC and X-FGPC. On the other hands, within the specific region of the core thickness, the value of the X-FGPC's elastic moduli becomes higher than that of O-FGPC's which is due to the type of pores dispersion in this region. Using the abovementioned properties, the elastic modulus of the FGPC can be formulated as:

$$\begin{bmatrix} S_{11}(z) \\ S_{55}(z) \end{bmatrix}^c = \begin{bmatrix} E(z)(1 - \nu^2(z))^{-1} \\ 0.5E(z)(1 + \nu(z))^{-1} \end{bmatrix}^c \tag{28}$$

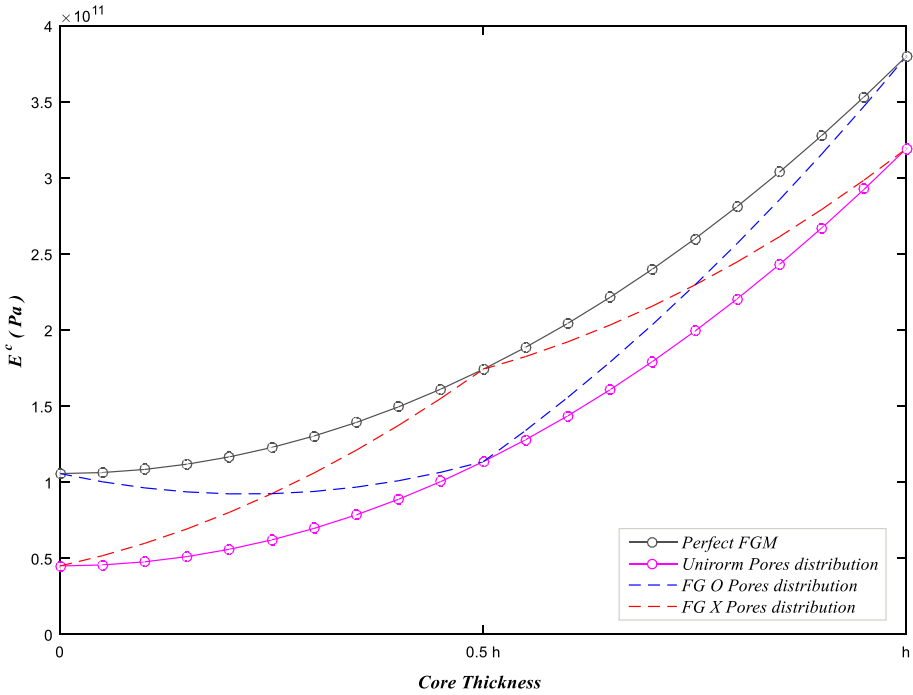


Fig. 4 The FGPC’s elastic moduli variation against its thickness for different types of pores dispersion

3 Governing Equations

Hamilton’s principle that serves as an energy-based technique is implemented to extract the governing equations of motion as (Arshid et al. 2020c):

$$\delta \int_{t_1}^{t_2} \{ \Psi + \Xi - \Gamma \} dt = 0 \tag{29}$$

where Ψ , Ξ , and Γ give a hint to the kinetic energy, externally applied work, and the strain energy, correspondingly.

The kinetic energy of the whole ESB can be derived as (Arshid and Khorshidvand 2018):

$$\Psi = 0.5 \int_x^{+h/2} \int_{-h/2}^{+h/2} \rho^{c,t,b}(z) \left[(U_{,t})^2 + (W_{,t})^2 \right] dz dx \tag{30}$$

The second term of Hamilton’s principle is the external work that is originated from the externally applied force due to the thermal environment affection. The thermal force in response to the addressed thermal surrounding is simulated as (Arshid et al. 2021c):

$$F_x^T = \int_{-h/2}^{+h/2} S_{11}^{c,t,b} \theta^{c,t,b} \Delta T dz, \quad (31)$$

The thermal external work can be simulated as (Arshid et al. 2019b):

$$\Xi = 0.5 \int_x F_x^T (w_x)^2 dx \quad (32)$$

Passing from the kinetic energy and the external work, the third part of Hamilton's principle equation addresses the strain energy of the ESB that becomes divided into two branches; classic strain energy of the beam and strain energy of the Vlasov's substrate.

The classical strain energy of the ESB will be derived using the following equation as (Amir et al. 2020b):

$$\Gamma_1 = 0.5 \int_x \int_{-h/2}^{+h/2} [\sigma_{xx} \varepsilon_x + \tau_{xz} \gamma_{xz}]^{c,t,b} dz dx \quad (33)$$

About foundation, it is better to mention a short background regarding Vlasov's foundation model and its properties, firstly. At the first time, Vlasov, to consider the vertical shearing parameter, based on the variational approach and also continuum principles progressed a bi-parameter novel foundation model that becomes famous as Vlasov's foundation. His model is assumed to be elastic, homogeneous, and isotropic. Furthermore, silica aerogel is assumed to play the role of constituting substrate material for under examination ESB. Based on Vlasov's foundation model and by considering a Cartesian coordinate system attached to the top surface of the substrate, the strain energy of substrate can be addressed as (Ghorbanpour Arani and Zamani 2019):

$$\Gamma_2 = 0.5 \int_{-\infty}^{+\infty} \int_{-H}^0 [\sigma_{xx} \varepsilon_{xx} + \sigma_{zz} \varepsilon_{zz} + \tau_{xz} \gamma_{xz}]^f dz dx, \quad (34)$$

In which H implies the foundation thickness and superscript f addresses Vlasov's foundation. Moreover, the related stress and strains can be defined by defining a new displacement field for the substrate as (Navarro et al. 2013):

$$\begin{aligned} \bar{U}(x, z, t) &= 0, \\ \bar{W}(x, z, t) &= w(x, t) \lambda(z) \end{aligned} \quad (35)$$

It should be noticed that the displacement in the x -direction is considered zero based on this assumption that its value is relatively negligible in comparison with vertical displacement. Also, λ is correlated with the shape function of the substrate with boundary conditions as:

$$\lambda(0) = 1, \quad \lambda(-H) = 0 \quad (36)$$

Accordingly, the foundation's stress and strain fields are presented as (Ghorbanpour Arani and Zamani 2018):

$$\begin{bmatrix} \varepsilon_{xx} \\ \varepsilon_{zz} \\ \gamma_{xz} \end{bmatrix}^f = \begin{bmatrix} \bar{U}_{,x} \\ \bar{W}_{,z} \\ \bar{U}_{,z} + \bar{W}_{,x} \end{bmatrix}, \begin{bmatrix} \sigma_{xx} \\ \tau_{xz} \\ \sigma_{zz} \end{bmatrix}^f = \begin{bmatrix} S_{11} & 0 & S_{13} \\ 0 & S_{22} & 0 \\ S_{31} & 0 & S_{33} \end{bmatrix}^f \begin{bmatrix} \varepsilon_{xx} \\ \gamma_{xz} \\ \varepsilon_{zz} \end{bmatrix}^f \tag{37}$$

In which S serves as the foundation elastic coefficient and can be defined as:

$$\begin{aligned} S_{11}^f = S_{33}^f &= \frac{(1 - \nu^f)E^f}{(1 + \nu^f)(1 - 2\nu^f)}, \\ S_{13}^f = S_{31}^f &= \frac{E^f \nu^f}{(1 + \nu^f)(1 - 2\nu^f)}, \\ S_{22}^f &= \frac{E^f}{2(1 + \nu^f)} \end{aligned} \tag{38}$$

Inserting Eq. (37) into Eq. (34) and its rewriting led the foundation strain energy formulation to the final format as:

$$\Gamma_2 = 0.5 \int_{-\infty}^{+\infty} \int_{-H}^0 \left[S_{33}^f (w_{\lambda,z})^2 + S_{22}^f (\lambda w_x)^2 \right] dz dx \tag{39}$$

This equation, by minimizing respect to w , is capable to transform to the differential type equation through mathematical considerations as (Navarro et al. 2013):

$$-L_1 \frac{\partial^2 w}{\partial x^2} + L_2 w = 0 \tag{40}$$

In which, L_1 and L_2 are the foundation parameters and address, respectively, the shear parameter of foundation and the compression parameter of foundation.

$$\begin{aligned} L_1 &= S_{22}^f \int_{-H}^0 \lambda^2 dz, \\ L_2 &= S_{33}^f \int_{-H}^0 (\lambda_z)^2 dz \end{aligned} \tag{41}$$

In which the shape function is presented as follows (Vallabhan et al. 1991):

$$\lambda(z) = \frac{\sinh \left[\Sigma \left(1 - \frac{z}{H} \right) \right]}{\sinh [\Sigma]}, \left(\frac{\Sigma}{H} \right)^2 = \frac{S_{22}^f \int_{-\infty}^{+\infty} (w_x)^2 dx}{S_{33}^f \int_{-\infty}^{+\infty} w^2 dx} \tag{42}$$

where Σ is the parameter correlated with the deformation of the core.

Finally, the net ESB's strain energy is catchable using the summation principle as:

$$\Gamma = \Gamma_1 + \Gamma_2 \tag{43}$$

Substituting Eqs. (30, 32, 43) into Eq. (29) and applying some mathematical manipulations as, districting integrals with respect to z and integrating by part, equations of motion can be obtained in the stress resultants terms as:

$$\delta u :$$

$$-\frac{\partial}{\partial x}N_{xx0} - J_0 \frac{\partial^2 u}{\partial t^2} - J_1 \frac{\partial^3 w}{\partial t^2 \partial x} - J_4 \frac{\partial^2 u_1}{\partial t^2} = 0, \quad (44)$$

$\delta u_1 :$

$$-\frac{\partial}{\partial x}N_{xx4} + N_{xz5} - J_4 \frac{\partial^2 u}{\partial t^2} + J_{14} \frac{\partial^3 w}{\partial t^2 \partial x} - J_{44} \frac{\partial^2 u_1}{\partial t^2} = 0, \quad (45)$$

$\delta w :$

$$-\frac{\partial^2}{\partial x^2}N_{xx1} - J_1 \frac{\partial^3 u}{\partial t^2 \partial x} + J_2 \frac{\partial^4 w}{\partial t^2 \partial x^2} - J_{14} \frac{\partial^3 u_1}{\partial t^2 \partial x} - J_0 \frac{\partial^2 w}{\partial t^2} - L_1 \frac{\partial^2 w}{\partial x^2} + L_2 w - F_x^T \frac{\partial^2 w}{\partial x^2} = 0 \quad (46)$$

In which:

$$\begin{aligned} [N_{xx0}, N_{xx1}, N_{xx4}] &= \int_{-\frac{h}{2}}^{\frac{h}{2}} \sigma_{xx} [1, z, f(z)] dz, \\ [N_{xz5}] &= \int_{-\frac{h}{2}}^{\frac{h}{2}} \sigma_{xz} \frac{\partial}{\partial z} f(z) dz \end{aligned} \quad (47)$$

By inserting some mathematical manipulation, the stress resultants can be defined as:

$$\begin{aligned} N_{xx0} &= S_{110} \frac{\partial u}{\partial x} - S_{111} \frac{\partial^2 w}{\partial x^2} + S_{114} \frac{\partial u_1}{\partial x}, \\ N_{xx1} &= S_{111} \frac{\partial u}{\partial x} - S_{112} \frac{\partial^2 w}{\partial x^2} + S_{1114} \frac{\partial u_1}{\partial x}, \\ N_{xx4} &= S_{114} \frac{\partial u}{\partial x} - S_{1114} \frac{\partial^2 w}{\partial x^2} + S_{1144} \frac{\partial u_1}{\partial x}, \\ N_{xz5} &= S_{555} u_1 \end{aligned} \quad (48)$$

In which:

$$\begin{aligned} [S_{110}, S_{111}, S_{112}, S_{114}] &= \int_{-\frac{h}{2}}^{\frac{h}{2}} S_{11} [1, z, z^2, f(z)] dz, \\ [S_{1114}, S_{1144}] &= \int_{-\frac{h}{2}}^{\frac{h}{2}} S_{11} [zf(z), f(z)^2] dz, \\ [S_{555}] &= \int_{-\frac{h}{2}}^{\frac{h}{2}} S_{55} \left[\frac{\partial f(z)}{\partial z} \right]^2 dz \end{aligned} \quad (49)$$

Also, coefficients related to the kinematic terms can be defined as:

$$\begin{aligned}
 J_0 &= \int_{-0.5h_c-h_b}^{-0.5h_c} \rho^b(z)dz + \int_{-0.5h_c}^{+0.5h_c} \rho^c(z)dz + \int_{+0.5h_c}^{+0.5h_c+h_t} \rho^t(z)dz, \\
 J_1 &= \int_{-0.5h_c-h_b}^{-0.5h_c} z\rho^b(z)dz + \int_{-0.5h_c}^{+0.5h_c} z\rho^c(z)dz + \int_{+0.5h_c}^{+0.5h_c+h_t} z\rho^t(z)dz, \\
 J_2 &= \int_{-0.5h_c-h_b}^{-0.5h_c} z^2\rho^b(z)dz + \int_{-0.5h_c}^{+0.5h_c} z^2\rho^c(z)dz + \int_{+0.5h_c}^{+0.5h_c+h_t} z^2\rho^t(z)dz, \\
 J_4 &= \int_{-0.5h_c-h_b}^{-0.5h_c} f(z)\rho^b(z)dz + \int_{-0.5h_c}^{+0.5h_c} f(z)\rho^c(z)dz + \int_{+0.5h_c}^{+0.5h_c+h_t} f(z)\rho^t(z)dz, \\
 J_{14} &= \int_{-0.5h_c-h_b}^{-0.5h_c} zf(z)\rho^b(z)dz + \int_{-0.5h_c}^{+0.5h_c} zf(z)\rho^c(z)dz + \int_{+0.5h_c}^{+0.5h_c+h_t} zf(z)\rho^t(z)dz, \\
 J_{44} &= \int_{-0.5h_c-h_b}^{-0.5h_c} f(z)^2\rho^b(z)dz + \int_{-0.5h_c}^{+0.5h_c} f(z)^2\rho^c(z)dz + \int_{+0.5h_c}^{+0.5h_c+h_t} f(z)^2\rho^t(z)dz
 \end{aligned} \tag{50}$$

4 Analytical Solution Procedure

Based on Navier’s solution technique, the governing equations are solved analytically. Regarding this technique, the geometrical boundary conditions for the simply supported type of beam become satisfied using the following expressions for displacement components as (Arshid et al. 2019c):

$$\begin{bmatrix} u(x, t) \\ u_1(x, t) \\ w(x, t) \end{bmatrix} = \sum_{m=1}^{\infty} \begin{bmatrix} U \cos(\chi x) \\ U_1 \cos(\chi x) \\ W \sin(\chi x) \end{bmatrix} e^{i\omega t} \tag{51}$$

where U , U_1 , and W serve as unknown coefficients. Also, $\chi = \frac{m\pi}{a}$ and m denotes the mode number along ESB’s length. For the sake of simplicity, the final formulation is capable to have a compact and matrixial expression as (Thai et al. 2015):

$$[A - B\omega^2]_{3*3}[\Lambda]_{3*1} = 0 \tag{52}$$

In the final formulation, A , B , and Λ address stiffness matrix, mass matrix, and displacement vector, correspondingly. The matrix A and B can be presented in detail as:

$$A = \begin{bmatrix} A_{11} & A_{12} & A_{13} \\ A_{21} & A_{22} & A_{23} \\ A_{31} & A_{32} & A_{33} \end{bmatrix}, B = \begin{bmatrix} B_{11} & B_{12} & B_{13} \\ B_{21} & B_{22} & B_{23} \\ B_{31} & B_{32} & B_{33} \end{bmatrix} \tag{53}$$

where

Table 2 ESB’s core constituents’ properties (Sharma et al. 2018)

Material	ρ (Kg/m ³)	ν	E (GPa)	θ (10 ⁻⁶ /K)
Al ₂ O ₃	3800	0.3	380	8.3
ZrO ₂	3000	0.3	151	10
Si ₃ N ₄	2370	0.24	322.27	5.87
Ti-6Al-4 V	4429	0.298	105.7	10.3
Al	2707	0.3	70	24
SUS304	8166	0.317	207.78	12.33

Table 3 ESB’s face sheets constituents’ properties (Moradi-Dastjerdi et al. 2020a)

Material	ρ (Kg/m ³)	E (GPa)	θ (10 ⁻⁶ /K)	K (GPa)	G (GPa)
PMMA	1150	2.5	45	2.6	0.93
CNF	1400	5646.6	3.45	–	–

$$\begin{aligned}
 [A_{11}, A_{12}, A_{13}] &= \chi^2 [S_{110}, S_{114}, -\chi S_{111}], \\
 [A_{21}, A_{22}, A_{23}] &= [\chi^2 S_{114}, \chi^2 S_{1144} + S_{5555}, -\chi^3 S_{1114}], \\
 [A_{31}, A_{32}, A_{33}] &= [-\chi^3 S_{111}, -\chi^3 S_{1114}, \chi^4 S_{112} + \chi^2 L_1 + L_2 + \chi^2 F_x^T], \\
 [B_{11}, B_{12}, B_{13}] &= [-J_0, -J_4, \chi J_1], \\
 [B_{21}, B_{22}, B_{23}] &= [-J_4, -J_{44}, \chi J_{14}], \\
 [B_{31}, B_{32}, B_{33}] &= [\chi J_1, \chi J_{14}, -\chi^2 J_2 - J_0]
 \end{aligned} \tag{54}$$

5 Numerical Results and Discussion

Passing from the abovementioned sections and formulations, in the current section, the vibrational responses of the ESB to the different variables’ variations are presented to accounts for their impacts on the current model’s vibrational behaviors. As mentioned previously, ESB is constituted from an FGPC and two ACNFRCs as face sheets. The thickness of the core, the thickness of each one of the face sheets, and the length of the model assumed to be 5 mm, 0.5 mm, and 20 mm, respectively. What’s more and for the sake of integrity, the effect of FGPC’s different materials’ utilization is considered in the current study. The properties of all used materials are collected and displayed in Table 2 (Sharma et al. 2018) and Table 3 (Moradi-Dastjerdi et al. 2020a).

Moreover, about Vlasov’s foundation, getting a glimpse of Eqs. (40–42), it can be concluded that deformation (w), through foundation’s parameters, depends on the Σ . Also, the magnitude of Σ is dependent on the w . So, as presented graphically by Fig. 5, an iterative technique is required to find the exact value of Σ .

Base on Fig. 5, at the first stage, Σ assumed to be equal to 2. Then, using Eqs. (40–41), foundation’s parameters become determined. Then, governing equations are solved, and w is evaluated mathematically. Using obtained w , the new magnitude of Σ becomes extracted. There are two possibilities in this stage;

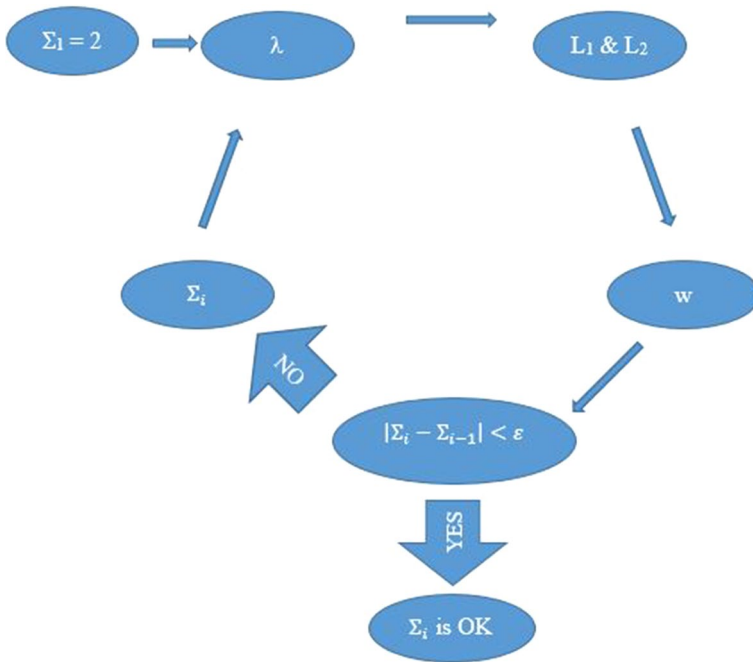


Fig. 5 The iterative technique procedure to determine the exact value of γ

- $|\Sigma_i - \Sigma_{i-1}| < \epsilon$. So, the new magnitude of Σ is reliable and based on this value substrate’s parameter becomes obtained and used in the solution of the governing equations.
- $|\Sigma_i - \Sigma_{i-1}| > \epsilon$. So, using the new magnitude of Σ the closed-loop circuit continues till the first condition become satisfied.

Furthermore, other mechanical and geometrical properties of the used Vlasov’s model are specified in Table 4 (Lei et al. 2013).

For the sake of the results’ reliability demonstration, Tables 5 and 6 are presented to compare the non-dimensional frequencies of the current model with their counterparts at the previously published works by Pagani et al. (2013) and Ghorbanpour Arani et al. (2018) according to various beam theories and mode numbers. For this reason, a beam with thickness $h=0.2\text{ m}$, length $a=2\text{ m}$, elastic modulus $E=75\text{GPa}$, density $\rho=2700\text{ kg/m}^3$ and Poisson’s ratio $\nu=0.33$ is considered.

As it is visible in the valid table, a good and close agreement among results elicited from the current formulation and those in the literature, guarantees the reliability of presented study exclusive results, truly. Also, the tiny differences among results can be due to the different software utilizations for the results obtaining. Furthermore, the way of code writing can be addressed as another reason for such a difference. From now on, the

Table 4 Mechanical and geometrical properties of Vlasov’s foundation (Lei et al. 2013)

Material	E (Pa)	ν	ρ (Kg/m ³)	H (mm)
Silica aerogel	$0.9638\rho^{3.378}$	$0.3236\rho^{-0.107}$	$300 < \rho < 1000$	30

Table 5 Validating the non-dimensional frequencies ($\varpi = \frac{\omega a^2}{h} \sqrt{\rho/E}$) of the current model with Pagani et al. (2013) based on the classic theory (CT) and FSDT for different mode numbers

	Mode No	Pagani et al. (2013)	Present
CT	1	2.885	3.007
	2	11.979	11.883
FSDT	1	2.885	2.971
	2	11.974	11.370

Table 6 Non-dimensional natural frequency ($\varpi = \frac{\omega a^2}{h} \sqrt{\rho/E}$) comparison between the current model results and those of Ghorbanpour Arani et al. (2018) based on the SSDT and different mode numbers

	Mode No	Ghorbanpour Arani et al. (2018)	Present
SSDT	1	2.963	2.964
	2	11.273	11.277

Table 7 The basic assumptions for the current paper exclusive results obtaining

FGPC's Material	ACNFRFC's Material	h_c (mm)	$h_t = h_b$ (mm)	a (mm)
Ti-6Al-4 V & Al ₂ O ₃	CNFs & PMMA	5	0.5	20
Ω	μ	η	f^*	n
$\omega a \sqrt{\rho_m/E_m}$	0.5	0.5	0.5	2
e	T _b (K)	m		
0.25	293	1		

Table 8 ESB's vibrational responses due to the various FGPC materials and different power-law exponents

n	Al			Ti-6Al-4 V			SUS304		
	Al ₂ O ₃	ZrO ₂	Si ₃ N ₄	Al ₂ O ₃	ZrO ₂	Si ₃ N ₄	Al ₂ O ₃	ZrO ₂	Si ₃ N ₄
0.5	6.1469	4.7542	6.6593	5.8610	4.5595	6.2244	5.4502	4.3374	5.6425
1	5.6339	4.5366	5.8764	5.2009	4.2486	5.3194	4.7375	4.0164	4.7673
2	4.9831	4.3001	5.0370	4.5118	3.9684	4.5153	4.1579	3.7872	4.1438
6	4.0176	4.0070	4.0110	3.6939	3.6807	3.6901	3.6085	3.5928	3.6069
7	3.9116	3.9781	3.9098	3.6146	3.6551	3.6156	3.5610	3.5771	3.5627
10	3.6992	3.9220	3.7121	3.4604	3.6067	3.4734	3.4715	3.5482	3.4801

main topic of discussion is about exclusive results of the under examination ESB which are obtained by considering presented assumptions in Table 7 as:

Table 8 illustrates the impacts of the power-law index and used materials in the FGPC on the vibrational behavior of ESB. This table states that the power-law index enhancement results in normalized frequency reduction which leads to a lower level of rigidity as an important physical and mechanical property. Furthermore, having a constant

power-law index, each ceramic cooperation with *Al* for FGPC formation addresses ESB more stiffness in comparison with that ceramic cooperation with other metals.

Figure 6 contains curvatures correlated with the vibrational responses to the various mode numbers and length to thickness ratio of the ESB. The curvatures imply a tremendous effect of the mode number enhancement which results in normalized frequency pushing up. As another output of this figure and from a physical point of view, it should be noted that by keeping ESB's total thickness constant and increasing its length continuously, the stiffness of the whole sandwich model decreases dramatically which causes the normalized frequency to fall as well. In accordance with provide a more touchable physical mindset, a ruler with different lengths can be assumed; it is obvious that the taller ruler is less stiff.

As mentioned before, Vlasov's foundation assumed as the elastic substrate in this paper. The effects of the foundation thickness and its elasticity moduli on the vibrational behavior of the current model are investigated in Fig. 7. As curvatures show, elasticity moduli and thickness of the Vlasov's substrate have an inverse impact on the normalized frequency and stiffness of the model; where the elasticity moduli enhancement and thickness reduction lead the whole structure to the more rigid and stiffer condition. Also, it is noticeable to mention that such a mentioned impact is more significant at the lower magnitudes of young modulus.

The influence and importance of the ACNFRFC face sheets' agglomeration degree on the frequential responses of the ESB are put under evaluation in Fig. 8. By the means of this figure, it is evident that the clusters' volume fraction (μ) elevation causes higher

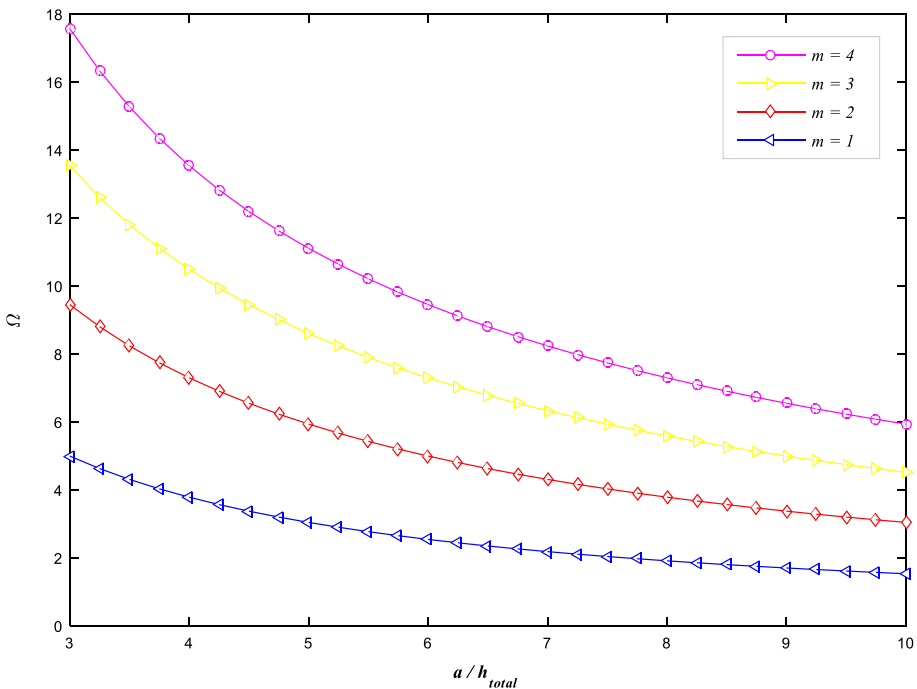


Fig. 6 Normalized frequency of the ESB versus length to thickness ratio at different mode numbers

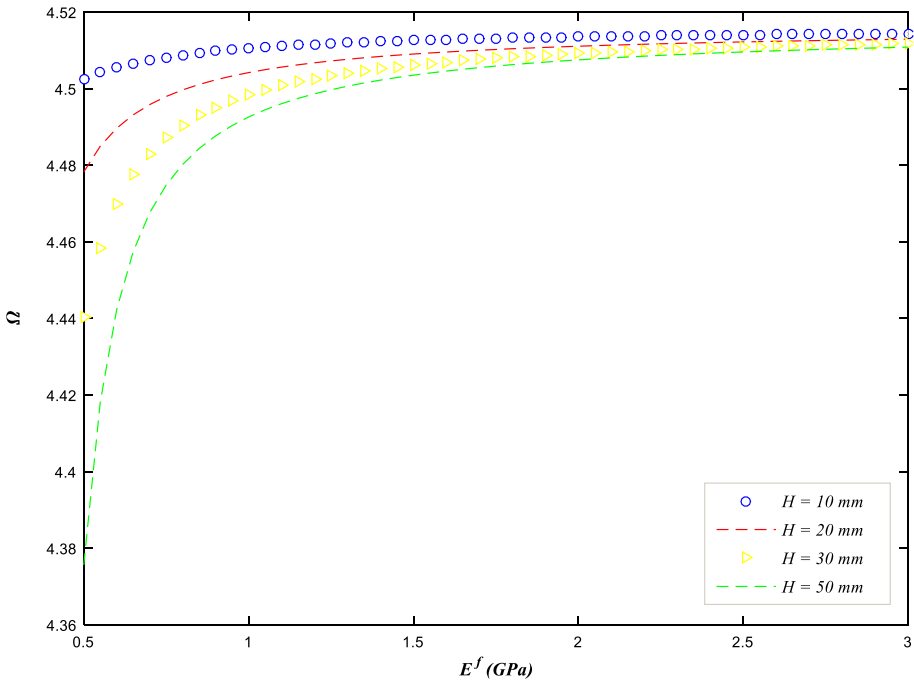


Fig. 7 The effects of the foundation thickness and its elasticity moduli on the vibrational behavior of the ESB

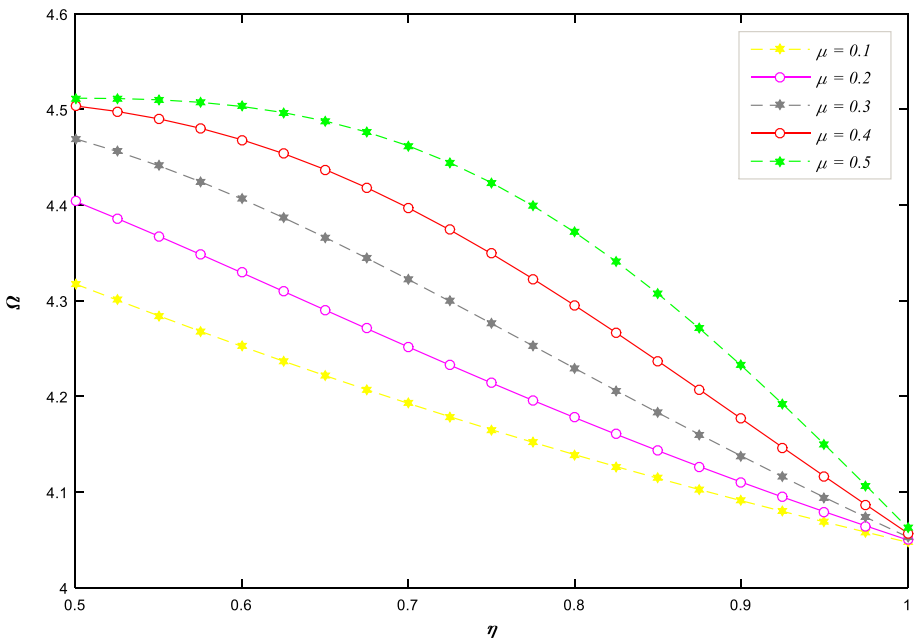


Fig. 8 The influence of the ACNFRCC face sheets' agglomeration degree on the frequential responses of the ESB

magnitudes of the normalized frequency and stiffness as follows. This result stresses the constructive effect of the agglomeration presence within the ACNFRFC top and bottom face sheet. On the other hands, it is proved that as the CNFs' volume fraction inside the clusters (η) becomes increased, the rigidity and stiffness of the model tend to decrease.

The current model is subjected to the thermal environment affection in which, the temperature varies linearly across the model's thickness. The bottom surface's temperature and ambient temperature are assumed to be equal to 300 K and 293 K, and also, the temperature variation across the z -direction is assumed to be linear. On the mentioned basis, Fig. 9 is concentrated on the vibrational behavior of the ESB model under variations of the temperature difference between the top and bottom surfaces and also, different face sheets' thickness. Using Fig. 9, it is demonstrated that as the top and bottom surfaces' temperature difference increases, the internal energy of the system enhances which, at the nano-scale, leads to the atomic bonding breakage. Furthermore, CNFs in nano-scale reinforce the material by the means of different mechanisms as bridging. By this mechanism, CNF forms a bridge between two granular materials. Increasing the temperature causes such a hardening mechanism to weaken and finally results in rigidity and stiffness loss. However, face sheets' thickness enhancement leads to the whole structure's thickness growth and finally, normalized frequency and stiffness growth as well. To originate an appropriate physical point of view, rulers with different thicknesses can be imagined. Which one is harder to bend?

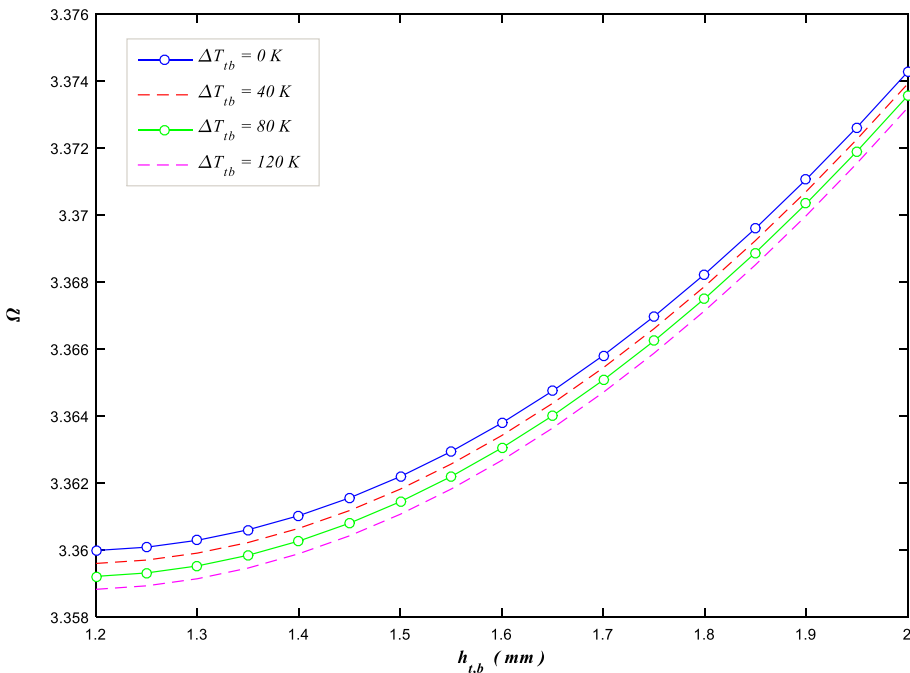


Fig. 9 Thermal environment effect on the normalized frequency of the sandwich model against ACNFRFC face sheets' thickness variations

Considering the uniform distribution of CNFs within the ACNFRCS, Fig. 10 stands to discuss the probability of ESB's mechanical behavior improvement by the means of appropriate.

FGPC's material and CNFs volume fraction (f^*) of the ACNFRCS. As it is displayed in this figure, higher values of f^* cause normalized frequency enhancement and, consequently, a higher level of rigidity of the sandwich model. In fact, by increasing the reinforcement phase the ability of the structure for carrying higher values of load enhances due to the high young modulus of CNFs. Secondly, based on Fig. 10, it is revealed that in an identical situation, the composition of *Al*, *Ti-6Al-4V*, and *SUS304* with Al_2O_3 as the FGPC's ingredients provides stiffer ESB, respectively.

Figure 11 is responsible to demonstrate ESB's vibrational behavior due to the material property exponent variations for the different displacement fields at the fourth mode. From a technical and analytical point of view, material property exponent increasing causes ceramic volume fraction reduction. As the ceramic young modulus is more than metal's young modulus considerably, it is rational that a stiffness reduction occurs by the ceramic volume fraction falling. Furthermore, as another result, it is proved that FSDT, HSDT, SSDT, and ESDT estimate the highest normalized frequency and rigidity for the sandwich prototype, one after another (Mohammadimehr et al. 2019). The difference between the results based on the FSDT and the results based on the other theories backs to the different types of shear deformation consideration in different theories. Therefore, by the means of FSDT, the effect of shear deformation is considered as a first-order/linear function of z . On the other hands, by the means of higher-order

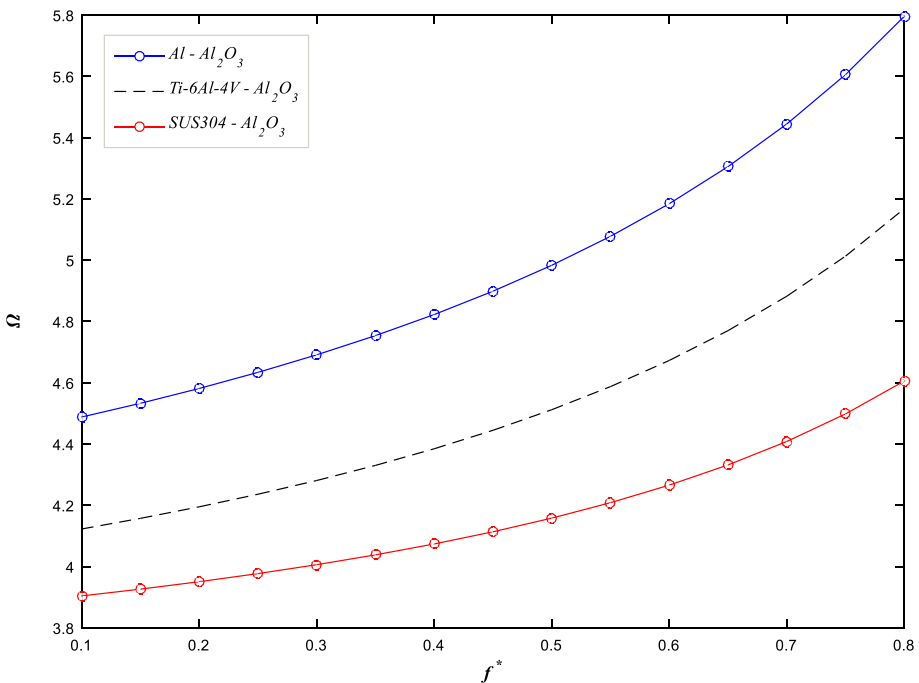


Fig. 10 Normalized frequency of the current ESB model versus CNFs volume fraction for different FGPC's materials

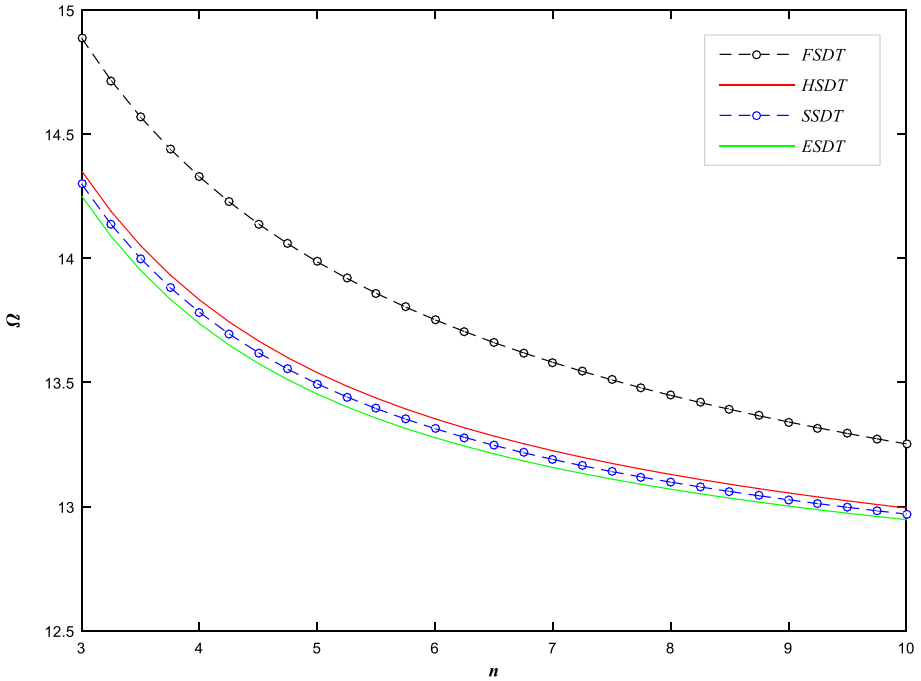


Fig. 11 The fourth mode normalized frequency against power-law exponent considering different displacement fields

theories, shear deformation impact is based on the nonlinear function of z . Such a non-linearity results in more complex equations and finally, a higher level of results' accuracy (Arshid et al. 2019a).

The influence of the different types of CNFs distribution within the ACFRCs on the ESB's stiffness at the fourth mode is investigated in Fig. 12. It is also important to mention that for CNFs distribution within the top and bottom ACFRC, the symmetry principle is respected. (i.e., whole under evaluation model is symmetrical to the mid-plane, even in CNFs distribution). According to the curvatures in this figure, the CNFs V-A pattern application provides the highest rigidity and consequently normalized frequency for the sandwich model. As the composite layers become thicker, the effect of CNF's distribution types on the normalized frequency becomes more considerable. That is why the difference among gained curves is more touchable in higher values of face sheets' thickness.

Figure 13 at the $m=4$ displays normalized frequency versus porosity-dependent parameters to survey their effects on the ESB's stiffness. Regarding Fig. 13, it can be observed that porosity index elevation results in density, normalized frequency, and stiffness reduction. Such an impact seems to be rational by imagining Cheetos or other porous materials in our surroundings. Furthermore, as curves say, the O type of pores dispersion addresses a higher level of rigidity in comparison with X type and uniform type of pores dispersions. Such behavior is due to the impact of different types of porosity dispersion on the mechanical properties of the model. The frequency magnitude is proportional to the second root of the stiffness (Young's modulus (E)) to density ratio.

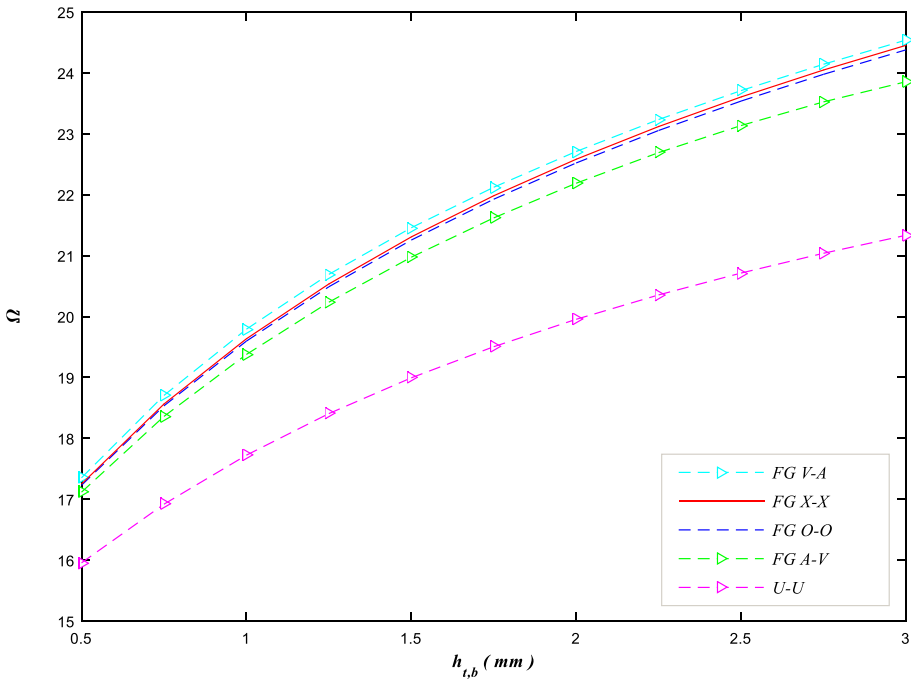


Fig. 12 The effect of the various CNFs distribution pattern within the ACNFRFC face sheets on the vibrational behavior of the sandwich beam

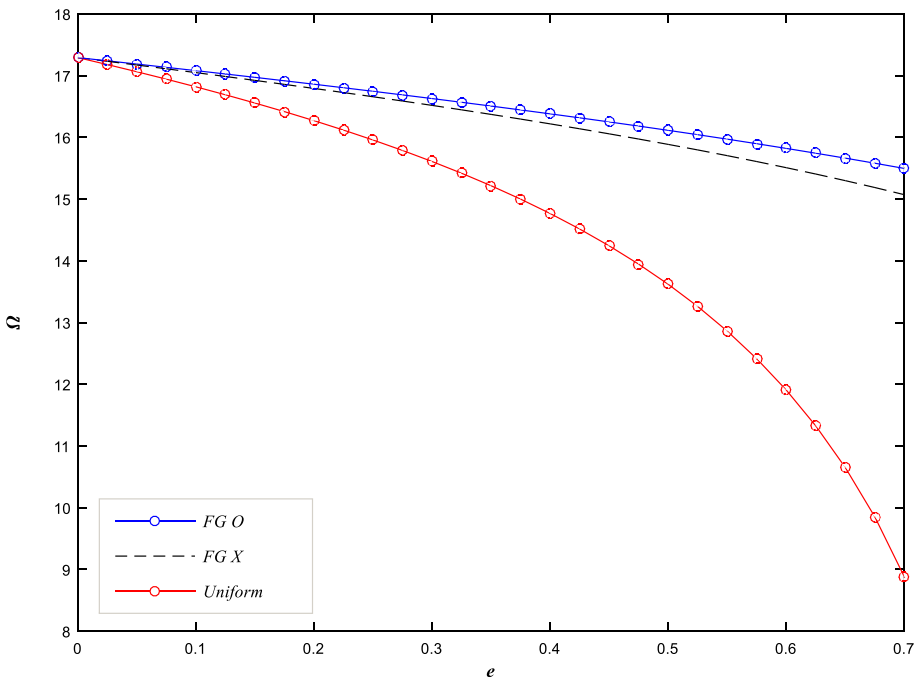


Fig. 13 Normalized frequency versus porosity-dependent parameters at the fourth mode

The mentioned ratio for O , X , and uniform type of pores dispersion captures the highest value, respectively. Also, by increasing the porosity index value, mentioned ratio's variation rate is more for uniform dispersion of pores, and consequently, the rate of the normalized frequency decreasing for the mentioned case is higher than two other types of pores' dispersion.

A three-dimensional diagram is presented by Fig. 14 to examine agglomerating and CNFs volume fraction effects on the normalized frequency of the ESB, simultaneously. To address the values more easily, Fig. 14 is presented as a bulk figure, but it should be noticed that the normalized frequency values are the surface values of the presented bulk figure. As it is obvious, both parameters' elevations have a constructive influence on the sandwich structures and lead it to a more rigid configuration.

6 Conclusion

In this paper, the authors proposed a challenge regarding the vibrational behavior of an equipped sandwich beam including two ACNFRFC face sheets and an FGPC on Vlasov's model substrate and also, under a thermal environment. The most considerable novelty of this work is the agglomeration impact application in the composite face sheets in such structures. In a conclusion, the clusters' presence in the composite face sheets plays a crucial constructive role in such sandwich structures' stiffness and rigidity. Furthermore, it is

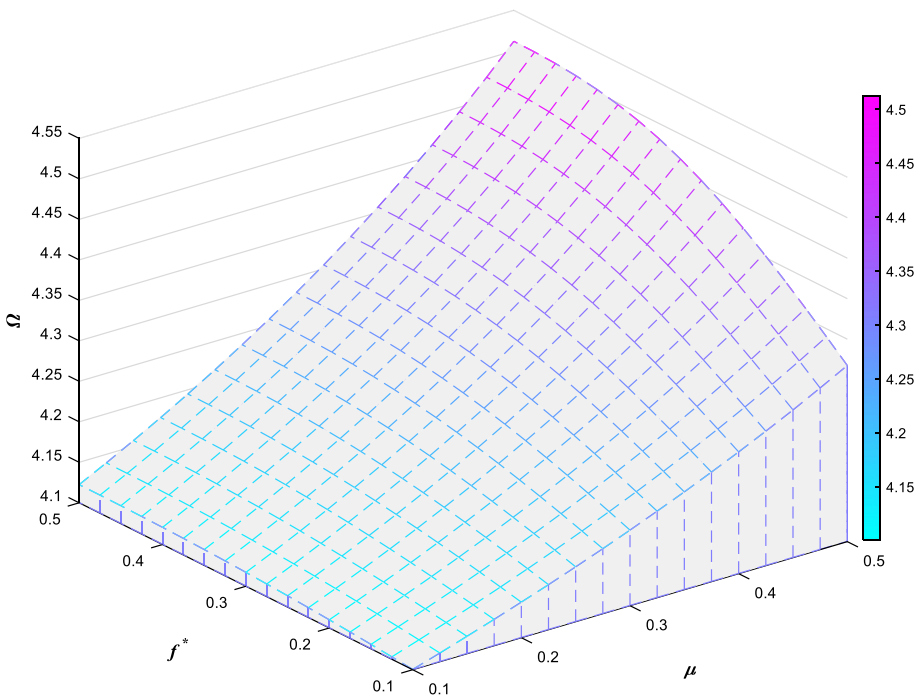


Fig. 14 The 3D diagram of the normalized frequency versus the CNFs volume fraction and agglomeration degree

proved that the CNFs V - A pattern application and porosities O pattern application provide the highest stiffness and consequently normalized frequency for the sandwich model over other types of CNFs' distribution and porosities dispersion. Also, it is concluded the Vlasov's substrate elasticity moduli and thickness enhancement have constructive and destructive impacts on the stiffness and normalized frequency of the aforementioned model, respectively. As another conclusion, it is worthwhile mentioning that Al & Si_3N_4 as the core material constituting and Timoshenko model of the beam predict higher stiffness of the whole structure in comparison with other materials and beam's theories. Furthermore, it is concluded that the sandwich model thickness and CNFs volume fraction have an identical impact on the normalized frequency and stiffness of the model (i.e., their enhancement in value results in stiffness enhancement and vice versa). To put it all in a nutshell, this paper seems to be helpful for future investigations in such a broad context.

Declarations

Conflict of interest The authors declare that they have no known competing financial interests or personal relationships that could have appeared to influence the work reported in this paper.

References

- Akbaş, Ş., Ersoy, H., Akgöz, B., Civalek, Ö.: Dynamic analysis of a fiber-reinforced composite beam under a moving load by the ritz method. *Mathematics* **9**, 1048 (2021). <https://doi.org/10.3390/math9091048>
- Akgöz, B., Civalek, Ö.: Thermo-mechanical buckling behavior of functionally graded microbeams embedded in elastic medium. *Int. J. Eng. Sci.* **85**, 90–104 (2014). <https://doi.org/10.1016/j.jjengsci.2014.08.011>
- Amir, S., Arshid, E., Ghorbanpour Arani, M.R.: Size-dependent magneto-electro-elastic vibration analysis of FG saturated porous annular/circular micro sandwich plates embedded with nano-composite face sheets subjected to multi-physical pre loads. *Smart Struct. Syst.* **23**, 429–447 (2019a)
- Amir, S., Soleimani-Javid, Z., Arshid, E.: Size-dependent free vibration of sandwich micro beam with porous core subjected to thermal load based on SSDBT. *Appl. Math. Mech.* (2019b). <https://doi.org/10.1002/zamm.201800334>
- Amir, S., Arshid, E., Khoddami Maraghi, Z.: Free vibration analysis of magneto-rheological smart annular three-layered plates subjected to magnetic field in viscoelastic medium. *Smart Struct. Syst.* **25**, 581–592 (2020a)
- Amir, S., Arshid, E., Khoddami Maraghi, Z., Loghman, A., Ghorbanpour Arani, A.: Vibration analysis of magnetorheological fluid circular sandwich plates with magnetostrictive facesheets exposed to monotonic magnetic field located on visco-Pasternak substrate. *J. Vib. Control.* **26**, 1523–1537 (2020b). <https://doi.org/10.1177/1077546319899203>
- Amir, S., BabaAkbar-Zarei, H., Khorasani, M.: Flexoelectric vibration analysis of nanocomposite sandwich plates. *Mech. Based. Des. Struct. Mach.* **48**, 146–163 (2020c). <https://doi.org/10.1080/15397734.2019.1624175>
- Arshid, E., Amir, S.: Size-dependent vibration analysis of fluid-infiltrated porous curved microbeams integrated with reinforced functionally graded graphene platelets face sheets considering thickness stretching effect. *Proc. Inst. Mech. Eng. Part. L J. Mater. Des. Appl.* (2021). <https://doi.org/10.1177/1464420720985556>
- Arshid, E., Khorshidvand, A.R., Khorsandijou, S.M.: The effect of porosity on free vibration of SPFG circular plates resting on visco-Pasternak elastic foundation based on CPT, FSDT and TSDT. *Struct. Eng. Mech.* **1**, 97–112 (2019a)
- Arshid, E., Kiani, A., Amir, S.: Magneto-electro-elastic vibration of moderately thick FG annular plates subjected to multi physical loads in thermal environment using GDQ method by considering neutral surface. *Proc. Inst. Mech. Eng. Part. L. J. Mater. Des. Appl.* **233**, 2140–2159 (2019b). <https://doi.org/10.1177/1464420719832626>

- Arshid, E., Kiani, A., Amir, S.: Asymmetric free vibration analysis of first-order shear deformable functionally graded magneto-electro-thermo-elastic circular plates. *Mech. Eng. Sci.* (2019c). <https://doi.org/10.1177/0954406219850598>
- Arshid, E., Amir, S., Loghman, A.: Static and dynamic analyses of FG-GNPs reinforced porous nanocomposite annular micro-plates based on MSGT. *Int. J. Mech. Sci.* (2020a). <https://doi.org/10.1016/j.ijmecsci.2020.105656>
- Arshid, E., Amir, S., Loghman, A.: Bending and buckling behaviors of heterogeneous temperature-dependent micro annular/circular porous sandwich plates integrated by FGPEM nano-Composite layers. *J. Sandw. Struct. Mater.* (2020b). <https://doi.org/10.1177/1099636220955027>
- Arshid, H., Khorasani, M., Soleimani-Javid, Z., Dimitri, R., Tornabene, F.: Quasi-3D hyperbolic shear deformation theory for the free vibration study of honeycomb microplates with graphene nanoplatelets-reinforced epoxy skins. *Molecules*. **25**, 5085 (2020c). <https://doi.org/10.3390/molecules25215085>
- Arshid, E., Amir, S., Loghman, A.: Thermal buckling analysis of FG graphene nanoplatelets reinforced porous nanocomposite MCST-based annular/circular microplates. *Aerosp. Sci. Technol.* (2021a). <https://doi.org/10.1016/j.ast.2021.106561>
- Arshid, E., Arshid, H., Amir, S., Mousavi, S.B.: Free vibration and buckling analyses of FG porous sandwich curved microbeams in thermal environment under magnetic field based on modified couple stress theory. *Arch. Civ. Mech. Eng.* (2021b). <https://doi.org/10.1007/s43452-020-00150-x>
- Arshid, E., Khorasani, M., Soleimani-Javid, Z., Amir, S., Tounsi, A.: Porosity-dependent vibration analysis of FG microplates embedded by polymeric nanocomposite patches considering hygrothermal effect via an innovative plate theory. *Eng. Comput* (2021c). <https://doi.org/10.1007/s00366-021-01382-y>
- Arshid, E., Khorshidvand, A.R.: Thin-walled structures free vibration analysis of saturated porous FG circular plates integrated with piezoelectric actuators via differential quadrature method. *Thin Walled Struct.* **125**, 220–233 (2018). <https://doi.org/10.1016/j.tws.2018.01.007>
- Avcar, M.: Free vibration of imperfect sigmoid and power law functionally graded beams. *Steel Compos. Struct.* **30**(6), 603–615 (2019). <https://doi.org/10.12989/scs.2019.30.6.603>
- Babaei, H., Eslami, M.R., Khorshidvand, A.R.: Thermal buckling and postbuckling responses of geometrically imperfect FG porous beams based on physical neutral plane. *J. Therm. Stress*. **43**, 109–131 (2019). <https://doi.org/10.1080/01495739.2019.1660600>
- Barati, M.R., Zenkour, A.M.: A general bi-Helmholtz nonlocal strain-gradient elasticity for wave propagation in nanoporous graded double-nanobeam systems on elastic substrate. *Compos. Struct.* **168**, 885–892 (2017). <https://doi.org/10.1016/j.compstruct.2017.02.0900263-8223>
- Civalek, Ö., Dastjerdi, S., Akbaş, Ş.D., Akgöz, B.: Vibration analysis of carbon nanotube-reinforced composite microbeams. *Math. Methods Appl. Sci.* (2021). <https://doi.org/10.1002/mma.7069>
- Dabbagh, A., Rastgoo, A., Ebrahimi, F.: Static stability analysis of agglomerated multi-scale hybrid nanocomposites via a refined theory. *Eng. Comput*. (2020a). <https://doi.org/10.1007/s00366-020-00939-7>
- Dabbagh, A., Rastgoo, A., Ebrahimi, F.: Thermal buckling analysis of agglomerated multiscale hybrid nanocomposites via a refined beam theory. *Mech. Based. Des. Struct. Mach.* (2020b). <https://doi.org/10.1080/15397734.2019.1692666>
- Daikh, A.A., Zenkour, A.M.: Free vibration and buckling of porous power-law and sigmoid functionally graded sandwich plates using a simple higher-order shear deformation theory. *Mater. Res. Express* **6**(11), 115707 (2019)
- Dastjerdi, S., Akgöz, B., Civalek, Ö.: On the effect of viscoelasticity on behavior of gyroscopes. *Int. J. Eng. Sci.* **149**, 103236 (2020). <https://doi.org/10.1016/j.ijengsci.2020.103236>
- Demir, C., Civalek, O.: On the analysis of microbeams. *Int. J. Eng. Sci.* **121**, 14–33 (2017). <https://doi.org/10.1016/j.ijengsci.2017.08.016>
- Duc, N.D., Seung-Eock, K., Tuan, N.D., Tran, P., Khoa, N.D.: New approach to study nonlinear dynamic response and vibration of sandwich composite cylindrical panels with auxetic honeycomb core layer. *Aerosp. Sci. Technol.* **70**, 396–404 (2017). <https://doi.org/10.1016/j.ast.2017.08.023>
- Fan, F., Sahmani, S., Safaei, B.: Isogeometric nonlinear oscillations of nonlocal strain gradient PFGM micro/nano-plates via NURBS-based formulation. *Compos. Struct.* **255**, 112969 (2021). <https://doi.org/10.1016/j.compstruct.2020.112969>
- Fantuzzi, N., Tornabene, F., Baccocchi, M., Dimitri, R.: Free vibration analysis of arbitrarily shaped functionally graded carbon nanotube-reinforced plates. *Compos. Part B Eng.* **115**, 384–408 (2017). <https://doi.org/10.1016/j.compositesb.2016.09.021>
- Foroutan, K., Carrera, E., Ahmadi, H.: Nonlinear hygrothermal vibration and buckling analysis of imperfect FG-CNTRC cylindrical panels embedded in viscoelastic foundations. *Eur. J. Mech. A/ solids*. **85**, 104107 (2021). <https://doi.org/10.1016/j.euromechsol.2020.104107>

- Fu, T., Wu, X., Xiao, Z., Chen, Z.: Thermoacoustic response of porous FGM cylindrical shell surround by elastic foundation subjected to nonlinear thermal loading. *Thin-Walled Struct.* **156**, 106996 (2020). <https://doi.org/10.1016/j.tws.2020.106996>
- Fu, T., Wu, X., Xiao, Z., Chen, Z.: Dynamic instability analysis of porous FGM conical shells subjected to parametric excitation in thermal environment within FSDT. *Thin-Walled Struct.* **158**, 107202 (2021a). <https://doi.org/10.1016/j.tws.2020.107202>
- Fu, T., Wu, X., Xiao, Z., Chen, Z.: Study on dynamic instability characteristics of functionally graded material sandwich conical shells with arbitrary boundary conditions. *Mech. Syst. Signal Process.* **151**, 107438 (2021b). <https://doi.org/10.1016/j.ymssp.2020.107438>
- Fu, T., Wu, X., Xiao, Z., Chen, Z.: Dynamic instability analysis of FG-CNTRC laminated conical shells surrounded by elastic foundations within FSDT. *Eur. J. Mech. A/Solids.* **85**, 104139 (2021c). <https://doi.org/10.1016/j.euromechsol.2020.104139>
- Fu, T., Wu, X., Xiao, Z., Chen, Z., Li, J.: Vibro-acoustic characteristics of eccentrically stiffened functionally graded material sandwich cylindrical shell under external mean fluid. *Appl. Math. Model.* **91**, 214–231 (2020d). <https://doi.org/10.1016/j.apm.2020.09.061>
- Ge, M., Zhao, Y., Huang, Y., Ma, W.: Static analysis of defective sandwich beam by Chebyshev quadrature element method. *Compos. Struct.* **261**, 113550 (2021). <https://doi.org/10.1016/j.compstruct.2021.113550>
- Ghorbanpour Arani, A., Zamani, M.H.: Bending analysis of agglomerated carbon nanotube-reinforced beam resting on two parameters modified Vlasov model foundation. *Indian J. Phys.* **92**, 767–777 (2018). <https://doi.org/10.1007/s12648-018-1162-z>
- Ghorbanpour Arani, A., Zamani, M.: Investigation of electric field effect on size-dependent bending analysis of functionally graded porous shear and normal deformable sandwich nanoplate on silica Aerogel foundation. *J. Sandw. Struct. Mater.* **21**, 2700–2734 (2019). <https://doi.org/10.1177/1099636217721405>
- Ghorbanpour Arani, A., BabaAkbar-Zarei, H., Pourmousa, P., Eskandari, M.: Investigation of free vibration response of smart sandwich micro-beam on winkler–pasternak substrate exposed to multi physical fields. *Microsyst. Technol.* **24**, 3045–3060 (2018). <https://doi.org/10.1007/s00542-017-3681-5>
- Jalaei, M., Civalek, O.: On dynamic instability of magnetically embedded viscoelastic porous FG nanobeam. *Int. J. Eng. Sci.* **143**, 14–32 (2019). <https://doi.org/10.1016/j.ijengsci.2019.06.013>
- Kamarian, S., Shakeri, M., Yas, M., Bodaghi, M., Pourasghar, A.: Free vibration analysis of functionally graded nanocomposite sandwich beams resting on Pasternak foundation by considering the agglomeration effect of CNTs. *J. Sandw. Struct. Mater.* **17**, 632–665 (2015). <https://doi.org/10.1177/1099636215590280>
- Kamarian, S., Salim, M., Dimitri, R., Tornabene, F.: Free vibration analysis of conical shells reinforced with agglomerated carbon nanotubes. *Int. J. Mech. Sci.* **108–109**, 157–165 (2016). <https://doi.org/10.1016/j.ijmecsci.2016.02.006>
- Khatua, T.P., Cheung, Y.K.: Bending and vibration of multilayer sandwich beams and plates. *Int. J. Numer. Methods Eng.* **6**, 11–24 (1973). <https://doi.org/10.1002/nme.1620060103>
- Khorasani, M., Soleimani-Javid, Z., Arshid, E., Lampani, L., Civalek, Ö.: Thermo-elastic buckling of honeycomb micro plates integrated with FG-GNPs reinforced Epoxy skins with stretching effect. *Compos. Struct.* **258**, 113430 (2021). <https://doi.org/10.1016/j.compstruct.2020.113430>
- Khorasani, M., Eyvazian, A., Karbon, M., Tounsi, A., Lampani, L., Sebaey, T.A.: Magneto-electro-elastic vibration analysis of modified couple stress-based three-layered micro rectangular plates exposed to multi-physical fields considering the flexoelectricity effects. *Smart Struct. Syst.* **26**, 331–343 (2020)
- Kumar, S., Renji, K.: Estimation of strains in composite honeycomb sandwich panels subjected to low frequency diffused acoustic field. *J. Sound Vib.* **449**, 84–97 (2019). <https://doi.org/10.1016/j.jsv.2019.02.013>
- Kumar, V., Singh, S.J., Saran, V.H., Harsha, S.P.: Vibration characteristics of porous FGM plate with variable thickness resting on Pasternak's foundation. *Eur. J. Mech. A/solids.* **85**, 104124 (2021). <https://doi.org/10.1016/j.euromechsol.2020.104124>
- Lazreg, H., Avcar, M.: Free vibration analysis of fg porous sandwich plates under various boundary conditions. *J. Appl. Comput. Mech.* **7**, 505–519 (2021a). <https://doi.org/10.22055/JACM.2020.35328.2628>
- Lazreg, H., Avcar, M.: Nonlocal free vibration analysis of porous FG nanobeams using hyperbolic shear deformation beam theory. *Adv. Nano Res.* **10**(3), 281–293 (2021b). <https://doi.org/10.12989/anr.2021.10.3.281>
- Le, C.I., Le, N.A.T., Nguyen, D.K.: Free vibration and buckling of bidirectional functionally graded sandwich beams using an enriched third-order shear deformation beam element. *Compos. Struct.* **261**, 113309 (2021). <https://doi.org/10.1016/j.compstruct.2020.113309>

- Leclaire, P., Horoshenkov, K.V., Cummings, A.: Transverse vibrations of a thin rectangular porous plate saturated by a fluid. *J. Sound Vib.* **247**, 1–18 (2001). <https://doi.org/10.1006/jsvi.2001.3656>
- Lei, J., Hu, J., Liu, Z.: Mechanical properties of silica aerogel - A molecular dynamics study. 2013 World Congr. Adv. Struct. Eng. Mech. 778–785 (2013)
- Maheri, M.R., Adams, R.D.: Steady-state flexural vibration damping of honeycomb sandwich beams. *Compos. Sci. Technol.* **52**, 333–347 (1994). [https://doi.org/10.1016/0266-3538\(94\)90168-6](https://doi.org/10.1016/0266-3538(94)90168-6)
- Mohammadimehr, M., Arshid, E., Rasti, S.M.A.: Free vibration analysis of thick cylindrical MEE composite shells reinforced CNTs with temperature - dependent properties resting on viscoelastic foundation. *Struct. Eng. Mech.* **6**, 683–702 (2019)
- Moradi-Dastjerdi, R., Behdinin, K., Safaei, B., Qin, Z.: Buckling behavior of porous CNT-reinforced plates integrated between active piezoelectric layers. *Eng. Struct.* (2020a). <https://doi.org/10.1016/j.engstruct.2020.111141>
- Moradi-Dastjerdi, R., Behdinin, K., Safaei, B., Qin, Z.: Static performance of agglomerated CNT-reinforced porous plates bonded with piezoceramic faces. *Int. J. Mech. Sci.* (2020b). <https://doi.org/10.1016/j.ijmecsci.2020.105966>
- Mousavi, S.B., Amir, S., Jafari, A., Arshid, E.: Analytical solution for analyzing initial curvature effect on vibrational behavior of PM beams integrated with FGP layers based on trigonometric theories. *Adv. Nano Res.* (2021). <https://doi.org/10.12989/anr.2021.10.3.235>
- Navarro, P., Abrate, S., Aubry, J., Marguet, S., Ferrero, J.-F.: Analytical modeling of indentation of composite sandwich beam. *Compos. Struct.* **100**, 79–88 (2013). <https://doi.org/10.1016/j.compstruct.2012.12.017>
- Pagani, A., Boscolo, M., Banerjee, J.R., Carrera, E.: Exact dynamic stiffness elements based on one-dimensional higher-order theories for free vibration analysis of solid and thin-walled structures. *J. Sound Vib.* **332**, 6104–6127 (2013). <https://doi.org/10.1016/j.jsv.2013.06.023>
- Sayyad, A.S., Ghugal, Y.M.: A sinusoidal beam theory for functionally graded sandwich curved beams. *Compos. Struct.* **226**, 111246 (2019). <https://doi.org/10.1016/j.compstruct.2019.111246>
- Sharma, A.K., Sharma, P., Chauhan, P.S., Bhadoria, S.S.: Study on harmonic analysis of functionally graded plates using FEM. *Int. J. Appl. Mech. Eng.* **23**, 941–961 (2018). <https://doi.org/10.2478/ijame-2018-0053>
- Shi, D., Feng, X., Huang, Y.Y., Hwang, K.-C., Gao, H.: The effect of nanotube waviness and agglomeration on the elastic property of carbon nanotube-reinforced composites. *J. Eng. Mater. Technol.* **126**, 250–257 (2004). <https://doi.org/10.1115/1.1751182>
- Şimşek, M., Reddy, J.N.: Bending and vibration of functionally graded microbeams using a new higher order beam theory and the modified couple stress theory. *Int. J. Eng. Sci.* **64**, 37–53 (2013). <https://doi.org/10.1016/j.ijengsci.2012.12.002>
- Sobhy, M.: Differential quadrature method for magneto-hydrothermal bending of functionally graded graphene/Al sandwich-curved beams with honeycomb core via a new higher-order theory. *J. Sandw. Struct. Mater.* (2020). <https://doi.org/10.1177/1099636219900668>
- Soleimani-Javid, Z., Arshid, E., Khorasani, M., Amir, S., Tounsi, A.: Size-dependent flexoelectricity-based vibration characteristics of honeycomb sandwich plates with various boundary conditions. *Adv. Nano Res.* **10**, 449–460 (2021). <https://doi.org/10.12989/anr.2021.10.5.449>
- Takahashi, D., Tanaka, M.: Flexural vibration of perforated plates and porous elastic materials under acoustic loading. *J. Acoust. Soc. Am.* **112**, 1456–1464 (2002). <https://doi.org/10.1121/1.1497624>
- Tang, Y., Ding, Q.: Nonlinear vibration analysis of a bi-directional functionally graded beam under hydrothermal loads. *Compos. Struct.* **225**, 111076 (2019). <https://doi.org/10.1016/j.compstruct.2019.111076>
- Thai, H.-T., Vo, T.P., Nguyen, T.-K., Lee, J.: Size-dependent behavior of functionally graded sandwich microbeams based on the modified couple stress theory. *Compos. Struct.* **123**, 337–349 (2015). <https://doi.org/10.1016/j.compstruct.2014.11.065>
- Thanh, C.-L., Tran, L.V., Bui, T.Q., Nguyen, H.X., Abdel-Wahab, M.: Isogeometric analysis for size-dependent nonlinear thermal stability of porous FG microplates. *Compos. Struct.* **221**, 110838 (2019). <https://doi.org/10.1016/j.compstruct.2019.04.010>
- Vallabhan, C.V.G., Straughan, W.T., Das, Y.C.: Refined model for analysis of plates on elastic foundation. *J. Eng. Mech.* **117**, 2830–2843 (1991)
- Zenkour, A.M.: Trigonometric solution for an exponentially graded thick plate resting on elastic foundations. *Arch. Mech. Eng.* **65**, 2193–2208 (2008). <https://doi.org/10.24425/123020>
- Zenkour, A.M.: Nonlocal elasticity and shear deformation effects on thermal buckling of a CNT embedded in a viscoelastic medium. *Eur. Phys. J. plus.* **133**, 196 (2018). <https://doi.org/10.1140/epjp/i2018-12014-2>
- Zenkour, M.: Quasi-3D refined theory for functionally graded porous plates: displacements and stresses. *Phys. Mesomech.* **23**, 39–53 (2020). <https://doi.org/10.1134/S1029959920010051>

- Zenkour, A.M., Radwan, A.F.: A nonlocal strain gradient theory for porous functionally graded curved nanobeams under different boundary conditions. *Phys. Mesomech.* **23**(6), 601–615 (2020). <https://doi.org/10.1134/S1029959920060168>
- Zenkour, A.M., Radwan, A.F.: A compressive study for porous FG curved nanobeam under various boundary conditions via a nonlocal strain gradient theory. *Eur. Phys. J. plus.* **136**, 248 (2021). <https://doi.org/10.1140/epjp/s13360-021-01238-w>
- Zhang, L.H., Lai, S.K., Wang, C., Yang, J.: DSC regularized dirac-delta method for dynamic analysis of FG graphene platelet-reinforced porous beams on elastic foundation under a moving load. *Compos. Struct.* **255**, 112865 (2021). <https://doi.org/10.1016/j.compstruct.2020.112865>

Publisher's Note Springer Nature remains neutral with regard to jurisdictional claims in published maps and institutional affiliations.